Peer-reviewed version available at *Inorganics* **2018**, *6*, 122; doi:10.3390/inorganics6040122

Hydrogenase biomimetics with redox-active ligands: Synthesis, structure and electrocatalytic studies on $Fe_2(CO)_4(\kappa^2$-dppn)(μ-edt) (edt = ethanedithiolate; dppn = 1,8-bis(diphenylphosphino)naphthalene)

Shishir Ghosh,[a,b,c,*] Shahed Rana,[b] Nathan Hollingsworth,[c] Michael G. Richmond,[d] Shariff E. Kabir[b] and Graeme Hogarth[a,*]

[a] Department of Chemistry, King's College London, Britannia House, 7 Trinity Street, London SE1 1DB, UK

[b] Department of Chemistry, Jahangirnagar University, Savar, Dhaka-1342, Bangladesh

[c] Department of Chemistry, University College London, 20 Gordon Street, London WC1H 0AJ, UK

[d] Department of Chemistry, University of North Texas, 1155 Union Circle, Box 305070, Denton, TX 76203, USA

E-mail: sghosh_006@yahoo.com (SG); graeme.hogarth@kcl.ac.uk (GH)

Abstract Addition of the bulky redox-active diphosphine 1,8-bis(diphenylphosphino)naphthalene (dppn) to $[Fe_2(CO)_6(\mu\text{-edt})]$ (**1**) (edt = 1,2-ethanedithiolate) affords $[Fe_2(CO)_4(\kappa^2\text{-dppn})(\mu\text{-edt})]$ (**3**) as the major product, together with small amounts of a P-C bond cleavage product $[Fe_2(CO)_5\{\kappa^1\text{-PPh}_2(1\text{-C}_{10}H_7)\}(\mu\text{-edt})]$ (**2**). The redox properties of **3** have been examined by cyclic voltammetry and it has been tested as a proton-reduction catalyst. It undergoes a reversible reduction at $E_{1/2} = -2.18$ V and exhibits two overlapping reversible oxidations at $E_{1/2} = -0.08$ V and $E_{1/2} = 0.04$ V. DFT calculations show that while the HOMO is metal-centred (Fe-Fe σ-bonding), the LUMO is primarily ligand-based but also contains an antibonding Fe-Fe contribution, highlighting the redox-active nature of the diphosphine. It is readily protonated upon addition of strong acids to afford two isomeric hydride complexes and catalyzes the electrochemical reduction of protons at $E_p = -2.00$ V in the presence of CF_3CO_2H. The catalytic current indicates that it is one of the most efficient diiron electrocatalysts for the reduction of protons, albeit operating at quite negative potential.

Keywords: Hydrogenase biomimetics; dithiolate; proton-reduction; dppn; redox-active

Peer-reviewed version available at *Inorganics* **2018**, *6*, 122; doi:10.3390/inorganics6040122

1. Introduction

Interest in of dithiolate-bridged diiron complexes [1-7] continues since they closely resemble the two-iron unit of the active site (H-cluster) of [FeFe]-hydrogenases [8,9]. Consequently over the past 20 years the synthesis, structural characterization and redox properties of a diverse range of diiron-dithiolate complexes has been studied [1-7,10-13], most focusing on their role as electrocatalysts for proton-reduction [14,15] but also in hydrogen oxidation [16-22]. Diphosphine complexes, $[Fe_2(CO)_4(\kappa^2\text{-diphosphine})(\mu\text{-dithiolate})]$, containing a chelating diphosphine are of special interest as they contain an unsymmetrical, redox-active, diiron centre and normally protonate rapidly to afford the corresponding hydride-cations, $[Fe_2(CO)_4(\mu\text{-H})(\kappa^2\text{-diphosphine})(\mu\text{-dithiolate})]^+$ [10-35]. Incorporation of redox-active ligands to the diiron center has also recently gained prominence [17,18,22,36-43] since the two redox systems can (potentially) interact electronically, acting in a cooperative manner [17,18,36] thus mimicking the communication relay between diiron and tetrairon sites that regulates enzyme activity [8,9,36,44,45]. Diphosphines bearing an extended π-system in their backbone such as 1,8-bis(diphenylphosphino)naphthalene (dppn) [46] and 2,3-bis(diphenylphosphino)maleic anhydride (bma) [47] are attractive surrogates of the tetrairon site due to the availability of a low-lying π^*-orbital delocalised over the ligand backbone. Their incorporation may both lower the reduction potential of the biomimetic by accommodating the incoming electron in the π^*-orbital, while also potentially facilitating electronic communication. Examples of diiron biomimetics containing these diphosphines are rare. In 2010, Schollhammer and co-workers reported studies on the bma complex, $[Fe_2(CO)_4(\mu\text{-pdt})(\kappa^2\text{-bma})]$, which has a relatively low reduction potential ($E_{1/2} = -0.89$ V); DFT studies showing that reduction is predominantly ligand-based [22]. Unfortunately, $[Fe_2(CO)_4(\mu\text{-pdt})(\kappa^2\text{-bma})]$ is inactive for proton-reduction, the lack of activity being attributed to the large gap between the redox potentials of the diiron and diphosphine sub-units thus retarding proton-coupled electron-transfer [22]. In 2011, Camara and Rauchfuss reported the dppn complex, $[Fe_2(CO)_4\{\mu\text{-}(SCH_2)_2NCH_2Ph\}(\kappa^2\text{-dppn})]$, and showed that its radical cation could catalyze hydrogen oxidation in the presence of an oxidant, being a thousand times faster than the related trisubstituted derivative, $[Fe_2(CO)_3(PMe_3)\{\mu\text{-}(SCH_2)_2NCH_2Ph\}(\kappa^2\text{-dppv})]^+$ [dppv = cis-1,2-bis(diphenylphosphino)ethylene] [16]. As far as we are aware, $[Fe_2(CO)_4\{\mu\text{-}(SCH_2)_2NCH_2Ph\}(\kappa^2\text{-dppn})]$ was not examined for its proton-reduction behaviour; indeed no diiron dppn complex has previously been examined in this

Peer-reviewed version available at Inorganics 2018, 6, 122; doi:10.3390/inorganics6040122

capacity. Consequently, herein we report the preparation and characterisation of the simple dppn complex, [$Fe_2(CO)_4(\kappa^2$-dppn)(μ-edt)] (**3**), together with an investigation of its proton-reduction ability.

2. Experimental

2.1. General Procedures

All reactions were carried out under a nitrogen atmosphere using standard Schlenk techniques. Reagent grade solvents were dried by the standard procedures and were freshly distilled prior to use. [$Fe_2(CO)_6$(μ-edt)] (**1**) was synthesized according to the literature procedure [48]. IR spectra were recorded on a Shimadzu FTIR 8101 spectrophotometer while the NMR spectra were recorded on a Bruker DPX 400 instrument. The chemical shifts were referenced to residual solvent resonances or external 85% H_3PO_4 in ^1H and ^{31}P spectra respectively. Elemental analyses were performed in the Microanalytical Laboratories of Wazed Miah Science Research Centre at Jahangirnagar University. Preparative thin layer chromatography was carried out on 1 mm plates prepared from silica gel GF254 (type 60, E. Merck) at Jahangirnagar University.

2.2. Synthesis

Me_3NO (21 mg, 0.279 mmol) was added to a MeCN solution (15 mL) of **1** (100 mg, 0.269 mmol) and dppn (134 mg, 0.270 mmol) and the mixture was heated to reflux for 1.5 h. After cooling to room temperature, volatiles were removed under reduced pressure and the residue chromatographed by TLC on silica gel. Elution with hexane/CH_2Cl_2 (4:1, v/v) developed three bands. The faster-moving band was unreacted **1** (trace). The second and third bands yielded [$Fe_2(CO)_5\{\kappa^1$-$PPh_2(1$-$C_{10}H_7)\}$(μ-edt)] (**2**) (14 mg, 8%) as red crystals and [$Fe_2(CO)_4(\kappa^2$-dppn)(μ-edt)] (**3**) (97 mg, 44%) as green crystals respectively after recrystallization from hexane/CH_2Cl_2 at 4 °C. Data for **2**: Anal. Calcd. for $C_{29}H_{21}Fe_2O_5PS_2$: C, 53.07; H, 3.23. Found: C, 53.81; H, 3.36%. IR (ν(CO), CH_2Cl_2): 2047s, 1985s, 1933w cm^{-1}. ^1H NMR ($CDCl_3$): δ 8.11 (d, J 8.4, 1H), 7.89 (m, 2H), 7.72 (m, 4H), 7.53 (t, J 7.6, 1H), 7.44 (m, 6H), 7.21 (m, 2H), 6.94 (dd, J 12.5, 7.6, 1H), 1.58 (m, 2H), 0.65 (m, 2H). $^{31}P\{^1H\}$ NMR ($CDCl_3$): δ 61.1 (s). Data for **3**: Anal. Calcd. for $C_{40}H_{30}Fe_2O_4P_2S_2$: C, 59.13; H, 3.72.

Peer-reviewed version available at Inorganics 2018, 6, 122; doi:10.3390/inorganics6040122

Found: C, 60.01; H, 3.86%. IR (ν(CO), CH_2Cl_2): 2021s, 1950m, 1901w cm^{-1}. ^{1}H NMR (CD_2Cl_2, 273 K): δ 8.11 (d, J 7.1, 2H), 7.65 (d, J 7.1, 8H), 7.38 (d, J 7.1, 6H), 7.31 (s, 2H), 7.17 (s, 8H), 1.87 (d, J 7.8, 2H), 1.29 (d, J 7.8, 2H). ^{31}P{^{1}H} NMR (CD_2Cl_2): δ 68.4 (s). ^{13}C{^{1}H} NMR (CD_2Cl_2, 233 K): δ 220.2 (t, J 19, CO), 215.7 (s, 2CO), 206.6 (s, CO), 141.1 (t, J 21), 137.2 (t, J 14), 135.9 (s), 135.7 (d, J 9), 135.0 (s), 133.4 (d, 30), 132.7 (s), 131.8 (t, J 19), 130.5 (d, J 23), 129.4 (s), 128.0 (s), 127.6 (s), 124.8 (s), 35.1 (s, Me). (CD_2Cl_2, 298 K) 220.3 (t, J 19, CO), 206.8 (br, 3CO). Other resonances not affected by temperature.

2.3. Protonation experiments

To a CH_2Cl_2 solution (*ca*. 2 mL) of **3** (made by dissolving 4.5 mg, 0.005 mmol) were added 2 molar equivalents of $HBF_4 \cdot Et_2O$. The resultant acid-containing solution was immediately transferred to an IR cell and monitored over time.

2.4. X-ray crystallography

Single crystals of **2** and **3** suitable for X-ray diffraction were grown by slow diffusion of hexane into a CH_2Cl_2 solution at 4 °C. All geometric and crystallographic data were collected at 150(2) K on a Bruker SMART APEX CCD diffractometer using Mo-Kα radiation (λ = 0.71073 Å) [49]. Data reduction and integration were carried out with SAINT+ [50] and absorption corrections were applied using the program SADABS [51]. The structures were solved by direct methods and refined by full-matrix least squares on F^2 [52]. All non-hydrogen atoms were refined anisotropically. The hydrogen atoms were placed in the calculated positions and their thermal parameters were linked to those of the atoms to which they were attached (riding model). The SHELXTL PLUS V6.10 program package was used for structure solution and refinement [52]. Final difference maps did not show any residual electron density of stereochemical significance. The details of the data collection and structure refinement are given in Table 1.

2.5. Electrochemical Studies

Electrochemistry was carried out either in deoxygenated MeCN with 0.1 M $TBAPF_6$ as the supporting electrolyte. The working electrode was a 3 mm diameter glassy carbon electrode that was polished with 0.3 µm alumina slurry prior to each scan. The counter electrode was a

Pt wire and the quasi-reference electrode was a silver wire. All CVs were referenced to the Fc^+/Fc redox couple. An Autolab potentiostat (EcoChemie, Netherlands) was used for all electrochemical measurements. Catalysis studies were carried out by adding equivalents of CF_3CO_2H (Sigma-Aldrich).

2.6. Computational methodology and modeling details

The DFT calculations were performed with the hybrid meta exchange-correlation functional M06 [53], as implemented by the Gaussian 09 program package [54]. The Fe [55] atoms were described by Stuttgart-Dresden effective core potentials (ecp) and an SDD basis set, while a 6-31G(d') basis set was employed for all second row elements and a 6-31G* basis set utilized for third row elements. The computed DFT structure for **3** represents a fully optimized ground state based on the positive eigenvalues displayed by the analytical Hessian.

3. Results and discussion

3.1. Synthesis and characterization

The Me_3NO-initiated reaction between $[Fe_2(CO)_6(\mu\text{-edt})]$ (**1**) and dppn in boiling MeCN gave two new diiron complexes; $[Fe_2(CO)_5\{\kappa^1\text{-}PPh_2(1\text{-}C_{10}H_7)\}(\mu\text{-edt})]$ (**2**) and $[Fe_2(CO)_4(\kappa^2\text{-dppn})(\mu\text{-edt})]$ (**3**) in 8 and 44% yield respectively (Scheme 1). While **3** was the anticipated product, isolation of **2** was unexpected since it results a carbon-phosphorus bond cleavage of dppn, generally requiring more extreme robust experimental conditions than those employed here. Complex **2** could be formed *via* direct reaction between **1** and Ph_2PNaph (possibly present as an impurity), however, we have no evidence of this as the purity of the dppn used was confirmed spectroscopically by $^{31}P\{^1H\}$ NMR. Dppn activation at di- and polynuclear carbonyl centres has precedent; formation of diphenyl(1-naphthyl)phosphine $\{PPh_2(1\text{-}C_{10}H_7)\}$, being previously reported by us and others [56, 57].

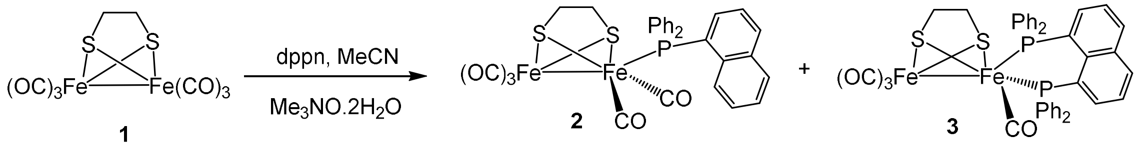

Scheme 1. Reaction of $[Fe_2(CO)_6(\mu\text{-edt})]$ (**1**) with dppn

Structural characterization of both **2** and **3** was made on the basis of the crystal structure as shown in Figs. 2 and 3 respectively The former contains a diiron core coordinated by five carbonyls, a Ph_2PNaph and a bridging edt ligand. The phosphine occupies an axial site, the Fe-P bond distance of 2.2442(6) Å being very similar to those reported for other $[Fe_2(CO)_5(\text{phosphine})(\mu\text{-edt})]$ complexes [29]. The Fe-Fe bond distance [2.5036(4) Å] is not affected by the phosphine substitution, being the same (within experimental error) as that in the parent hexacarbonyl **1** [2.5032 (5) Å] [58]. Spectroscopic data indicate that the solid-state structure persists in solution. The carbonyl region of the IR spectrum shows a characteristic absorptions pattern for $[Fe_2(CO)_5(\text{phosphine})(\mu\text{-dithiolate})]$ complexes, while the $^{31}P\{^1H\}$ NMR spectrum displays a singlet at 61.1 ppm. The ^1H NMR spectrum is not very informative, but shows two multiplets centred at 1.58 and 0.65 ppm (each integrating to two protons) attributed to the methylene protons of the edt-bridge, in addition to naphthyl and phenyl proton resonances in the aromatic region.

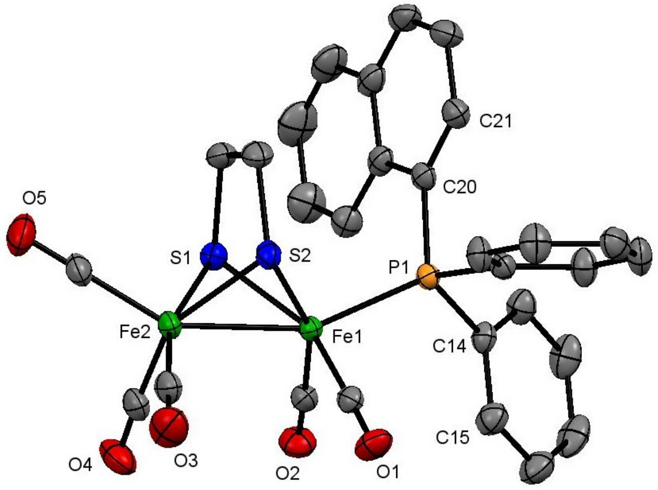

Fig. 1 Molecular structure of $[Fe_2(CO)_5\{\kappa^1\text{-}PPh_2(1\text{-}C_{10}H_7)\}(\mu\text{-edt})]$ (**2**) showing 50% probability thermal ellipsoids. Hydrogen atoms are omitted for clarity. [Selected bond distances (Å) and angles (°): Fe(1)─Fe(2) 2.5036(4), Fe(1)─P(1) 2.2442(6), Fe(1)─S(1) 2.2501(6), Fe(1)─S(2) 2.2611(6), Fe(2)─S(1) 2.2520(6),

Fe(2)─S(2) 2.2470(6); P(1)─Fe(1)─Fe(2) 155.755(18), P(1)─Fe(1)─S(1) 107.76(2), P(1)─Fe(1)─S(2) 106.08(2), P(1)─Fe(1)─C(1) 96.08(6), P(1)─Fe(1)─C(2) 95.55(6)].

The molecular structure of **3** is complicated by the existence of two independent molecules in the asymmetric unit linked via π-interactions of the naphthalene backbones [C(39)-C(40) and C(76)-C(77) C…C 3.271-3.633 Å]. Both independent molecules are similar (bond lengths and angles do not differ significantly) consisting of a diiron framework coordinated by four carbonyls, a chelating dppn, and an edt ligand which bridges the diiron centre. The Fe(1)─Fe(2) bond distance [2.5377(8) Å] is slightly elongated as compared to that of the parent hexacarbonyl **1** [2.5032 (5) Å] [58] probably in order to minimize the steric strain that accompanies dppn chelation. The dppn ligand is bound to Fe(1) occupying the apical and one of the basal coordination sites in the solid-state with a bite angle of 88.14(3)°. The Fe─P bond distances [Fe(1)─P(1) 2.1756(9) and Fe(1)─P(2) 2.1970(9) Å] are slightly shorter than that observed in **2**, but are within the range reported for related [$Fe_2(CO)_4(\kappa^2$-diphosphine)(μ-dithiolate)] complexes [22-27,29-35]. Solution spectroscopic data of **3** are consistent with the solid-state structure. The IR spectrum shows three absorptions at 2021s, 1950m, 1901w cm^{-1} for the carbonyls, while the $^{31}P\{^1H\}$ NMR spectrum displays only a singlet at 68.4 ppm. The ^1H NMR spectrum shows two doublets at 1.87 and 1.29 (J 7.8 Hz) ppm, each of which integrated for two protons, for the methylene protons of the edt-bridge in addition to naphthyl and phenyl proton resonances in the aromatic region. The $^{13}C\{^1H\}$ NMR spectrum at room temperature shows a broad resonance at 206.8 ppm attributed to the three carbonyls on the unsubstituted iron centre, and a sharp triplet at 220.3 ppm (J_{P-C} 19 Hz) for the fourth carbonyl. Upon cooling to -50 °C the broad resonance splits into two sharp singlets at 215.7 and 206.6 ppm (ratio 2:1) consistent with freezing out of the trigonal rotation of the $Fe(CO)_3$ moiety. No change is seen to the other carbonyl resonance and the $^{31}P\{^1H\}$ NMR spectrum broadens only slightly at -50 °C showing that interconversion of axial and equatorial phosphorus sites remains rapid even at this temperature.

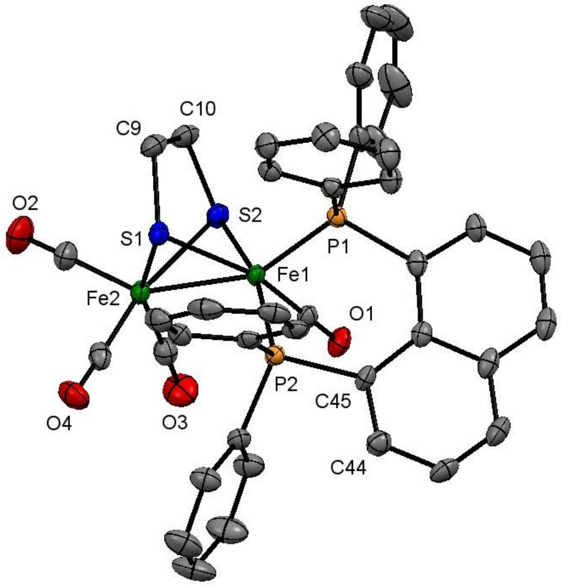

Fig. 2 Molecular structure of one independent molecule of [$Fe_2(CO)_6(\kappa^2$-dppn)(μ-edt)] (**3**) showing 50% probability thermal ellipsoids. Hydrogen atoms are omitted for clarity. [Selected bond distances (Å) and angles (°): Fe(1)─Fe(2) 2.5377(8), Fe(1)─P(1) 2.1756(9), Fe(1)─P(2) 2.1970(9), Fe(1)─S(1) 2.2478(9), Fe(1)─S(2) 2.2475(9), Fe(2)─S(1) 2.2526(9), Fe(2)─S(2) 2.2575(9); P(1)─Fe(1)─Fe(2) 155.21(3), P(2)─Fe(1)─Fe(2) 109.71(3), P(1)─Fe(1)─P(2) 88.14(3), P(1)─Fe(1)─S(1) 105.86(4), P(1)─Fe(1)─S(2) 107.90(3), P(1)─Fe(1)─C(1) 95.91(10)].

3.2. Protonation

Addition of a slight excess of $HBF_4{\cdot}Et_2O$ to a CH_2Cl_2 solution of **3** resulted in the immediate consumption of the latter as shown by IR spectroscopy. The appearance of new bands relating to two cationic hydrides was apparent as identified as dibasal [$Fe_2(CO)_4$(μ-H)(κ^2-dppn)(μ-edt)][BF_4] (**3bb**) (2081s, 2021vs, 1950m, 1898w cm^{-1}) and apical-basal [$Fe_2(CO)_4$(μ-H)(κ^2-dppn)(μ-edt)][BF_4] (**3ab**) (2097vs, 2040s, 1981m, 1890w cm^{-1}). Over time, absorptions associated with **3bb** diminished with concomitant growth of the ν(CO) bands for **3ab**. The rate of isomerization was dependent on acid concentration, being slower at low concentrations. With *ca.* 5 stoichiometric amounts of acid, immediate removal of excess acid and volatiles followed by washing in Et_2O allowed a clean IR spectrum of **3bb** to be obtained. Attempts to observe the cationic hydrides *via* NMR spectroscopy were unsuccessful but it is clear from the IR data that they are formed quickly and cleanly.

Peer-reviewed version available at *Inorganics* **2018**, *6*, 122; doi:10.3390/inorganics6040122

3.3. Electrochemistry

Complex **3** has been investigated by cyclic voltammetry (CV) in MeCN which shows a reversible reduction wave at $E_{1/2}$ = –2.18 V (ΔE = 80 mV) and two overlapping reversible oxidative waves at $E_{1/2}$ = –0.08 V (ΔE = 80 mV) and $E_{1/2}$ = 0.04 V (ΔE = 60 mV) (Fig. 3). The CV does not show any discernable change when the scan rate is varied (Fig. S1). The reduction wave also shows good chemical reversibility ($i_p^{ox}/\ i_p^{red}$ = ~0.85), and plots of reductive and oxidative peak currents of this reversible process against the square root of the scan rate give straight lines in support of a diffusion-controlled process on the CV time scale (Fig. S2). The current function ($i_p/\sqrt{\nu}$) associated with reduction deviates from linearity only at slow scan rates (< 0.05 V/s), indicating that more than one electron may be involved in reduction at longer time scales (Fig. S3); otherwise reduction of **3** is a one-electron process in MeCN. It is reduced at a similar potential to related [$Fe_2(CO)_4$(κ^2-diphosphine)(μ-dithiolate)] complexes containing non redox inactive diphosphines [26,27,30] which suggests that reduction is diiron-centered (as confirmed by DFT). Overlap of the two oxidative waves indicates that either the electrons are coming from separate parts of the same molecule, otherwise considerable gap would be seen between the two oxidation peaks, or **3** undergoes solvolysis after first oxidation to form probably [$Fe_2(CO)_3$(MeCN)(κ^2-dppn)(μ-edt)]$^+$ which reduces at the second oxidation potential. We can rule out the solvolysis because it would render the first oxidation wave irreversible.

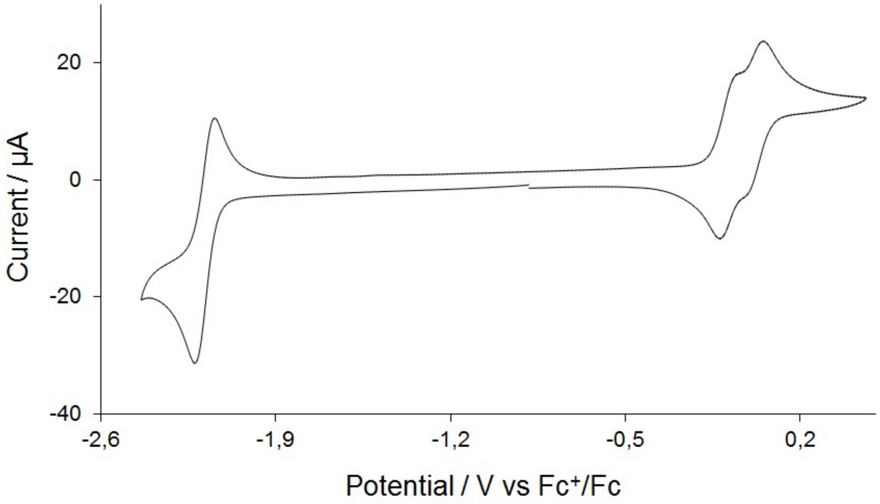

Fig. 3. CV of [$Fe_2(CO)_6$(κ^2-dppn)(μ-edt)] (**3**) in MeCN (1 mM solution, supporting electrolyte [NBu_4][PF_6], scan rate 0.1 Vs^{-1}, glassy carbon electrode, potential vs. Fc^+/Fc).

Peer-reviewed version available at *Inorganics* **2018**, *6*, 122; doi:10.3390/inorganics6040122

The nature of the HOMO and LUMO in **3** (Fig. 4) was evaluated by DFT in order to better understand the role the dppn ligand plays, if any, in the observed reduction of proton to H_2 (*vide infra*). The structure of **3** was optimized, and the geometry-optimized structure (not shown) revealed excellent agreement with the experimentally determined structure depicted in Fig. 2. The HOMO for **3** (left) is localized over the two iron centers and is best viewed as an in-phase Fe-Fe bond. The LUMO for **3** (right) exhibits the expected antibonding Fe-Fe interaction found in related derivatives along with a significant orbital contribution from the naphthalene π system, whose π* nodal properties are evident. The composition of the LUMO is best described as a ligand-based that contains an antibonding Fe-Fe contribution. The nodal pattern of the naphthalene π* in the LUMO of **3** is comparable to the LUMO computed for the cluster $[Fe_4(CO)_{10}(\kappa^2\text{-dppn})(\mu_4\text{-O})]$ [59]. The dppn π* system makes a much smaller contribution to the LUMO in the Fe_4 cluster relative to the antibonding metallic core. The enhanced catalytic behavior exhibited by **3**, vis-à-vis related derivatives of $[Fe_2(CO)_4(\kappa^2\text{-diphosphine})(\mu\text{-dithiolate})]$ whose ancillary diphosphine ligand does not contribute to the LUMO, signals the importance of the redox-active dppn ligand in promoting effective proton reduction.

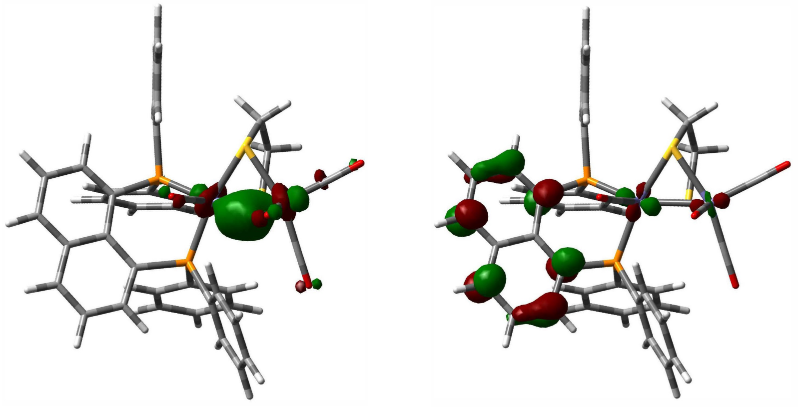

Fig. 4. Plots of the HOMO (left) and LUMO (right) of $[Fe_2(CO)_6(\kappa^2\text{-dppn})(\mu\text{-edt})]$ (**3**) as computed by DFT. Both plots were printed at an isovalue of 0.06. For the M06-optimized structure of **3**, we have utilized the Stuttgart-Dresden effective core potential and SDD basis set for the iron atoms and a 6-31G(d’) basis set for the remaining non-metal atoms.

Peer-reviewed version available at Inorganics 2018, 6, 122; doi:10.3390/inorganics6040122

3.4. Catalysis

Complex **3** was tested as a proton reduction catalyst in the presence of CF_3CO_2H in MeCN solvent (Figs. 5 and S4). Selected CVs recorded upon sequential addition of 1-7 molar equivalents of acid are shown in Fig. 5. Four new peaks are confirmed at E_p = -2.00, -2.11, -2.21 and -2.34 V in the CV after addition of one molar equivalent of acid. The peaks at E_p = -2.21 and -2.34 V are diminished as the acid concentration is increased and at high acid concentration (≥ 4 molar equivalents) only two peaks are observed. The protonation studies (*vide supra*) indicate that **3** forms two isomeric cationic hydride complexes assigned to **3ab** and **3bb** in the presence of acid, with the latter slowly converting into the former at low acid concentration. The **3bb** → **3ab** isomerization is sensitive to the concentration of added acid and the process is accelerated at high acid concentrations. This explains the observation of four peaks in the CV at low acid concentration. The height of the peaks at E_p = -2.00 and -2.11 increase with acid concentration and is characteristic of electrocatalytic proton reduction by this complex at these potentials. It appears that **3** enters into the catalytic cycle *via* a chemical step (protonation), followed by an electrochemical reduction which generates the neutral 35-electron complex $[Fe_2(CO)_4(\mu\text{-H})(\kappa^2\text{-dppn})(\mu\text{-edt})]$. This neutral hydride can either protonate or undergo a further reduction before a second protonation to liberate hydrogen. A plot of catalytic current/noncatalytic current ratio (i_{cat}/i_p) against concentration of acid is shown in Fig. 6 for the first catalytic wave. The i_{cat}/i_p value increases to 20 after addition of 10 equivalents CF_3CO_2H. To our knowledge very few biomimetic diiron systems developed as models of the active site of [FeFe]-hydrogenases show such high i_{cat}/i_p value [14,19,20,60]. For example, $[Fe_2(CO)_5(\kappa^1\text{-IMes})(\mu\text{-pdt})]$ [IMes = 1,3-bis(2,4,6-trimethylphenyl)imidazol-2-ylidene] which undergoes a two-electron reduction at –1.90 V vs. SCE shows an i_{cat}/i_p value of ~4 after addition of 10 molar equivalents of CH_3CO_2H [60,61]. The i_{cat}/i_p value serves as a measure the catalyst efficiency [60,62,63] and the values observed for **3** indicate that it is very efficient for the reduction of protons to H_2 although it operates at very negative potential (–2.00 V). The highest i_{cat}/i_p value observed to date for electrocatalytic proton reduction is 38 shown by the nickel complex $[(P^{Ph}{}_2N^{Ph})Ni]^{2+}$ ($P^{Ph}{}_2N^{Ph}$ = 1,3,6-triphenyl-1-aza-3,6-diphosphacycloheptane) [64].

Peer-reviewed version available at *Inorganics* **2018**, *6*, 122; doi:10.3390/inorganics6040122

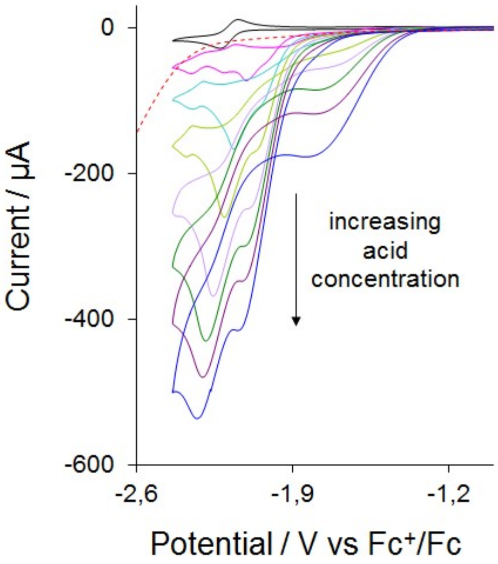

Fig. 5. CVs of [$Fe_2(CO)_6(\kappa^2$-dppn)(μ-edt)] (**3**) in the absence of acid and in the presence of 1-7 equivalents of CF_3CO_2H (in MeCN, 1 mM solution, supporting electrolyte [NBu_4][PF_6], scan rate 0.1 Vs^{-1}, glassy carbon electrode, potential vs Fc^+/Fc). Response of 10 equivalents CF_3CO_2H alone is shown with the red dotted line.

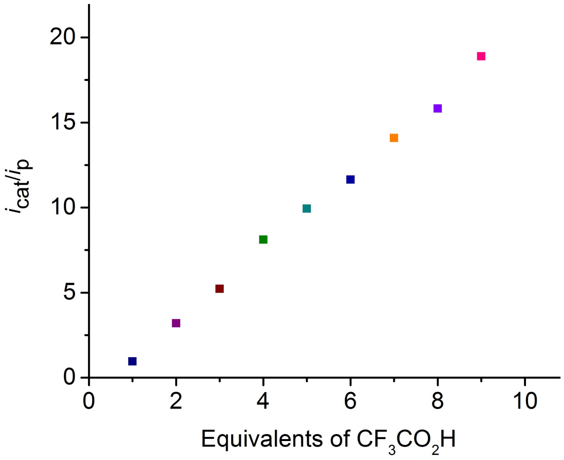

Fig. 6. Dependence of i_{cat}/i_p on CF_3CO_2H concentration for [$Fe_2(CO)_6(\kappa^2$-dppn)(μ-edt)] (**3**) at potentials of the first catalytic wave (in MeCN, 1 mM solution, 1-10 equivalents CF_3CO_2H, supporting electrolyte [NBu_4][PF_6], scan rate 0.1 Vs^{-1}, glassy carbon electrode).

4. Summary and conclusions

The diiron-dithiolate [$Fe_2(CO)_4(\kappa^2$-dppn)(μ-edt)] (**3**) containing a chelating dppn ligand has been synthesized from the reaction between [$Fe_2(CO)_6$(μ-edt)] (**1**) and dppn, a side product

$[Fe_2(CO)_5\{\kappa^1\text{-}PPh_2(1\text{-}C_{10}H_7)\}(\mu\text{-edt})]$ (**2**) resulting from P-C bond cleavage. Both **2** and **3** have been characterized by single-crystal X-ray diffraction analysis and structural features are unexceptional. DFT calculations on **3** show that while the HOMO is based exclusively at the diiron centre, the LUMO has a significant contribution from the naphthalene π-system showing that the dppn ligand is an integral part of the redox system. Cyclic voltammetry reveals that it undergoes a reversible part ligand based reduction and displays two overlapping reversible metal-centred oxidations in MeCN. Control experiments confirm that **3** is readily protonated in the presence of acid to give the cationic hydrides identified as dibasal $[Fe_2(CO)_4(\mu\text{-}H)(\kappa^2\text{-dppn})(\mu\text{-edt})][BF_4]$ (**3bb**) and apical-basal $[Fe_2(CO)_4(\mu\text{-}H)(\kappa^2\text{-dppn})(\mu\text{-edt})][BF_4]$ (**3ab**); the former hydride is less stable and transforms into the latter hydride over time. Complex **3** has been examined as an electrocatalyst for proton-reduction. Analysis of electrocatalytic data indicates that it operates at very negative potential (ca. -2 V) showing that even after protonation, reduction is primarily ligand based. However, that it is an active catalyst shows that there must be electronic communication between the dppn and diiron centres. Indeed, **3** is one of the most efficient diiron biomimetics reported to date and thus intramolecular electron-transfer within the cationic dihydride must be efficient. Thus the redox-active dppn ligand plays a critical role in the observed electrochemical proton-reduction. The exact nature of this remains unknown and in future work we will aim to better understand and exploit this electron coupling.

Acknowledgements

We thank the Commonwealth Scholarship Commission for the award of a Commonwealth Scholarship to S.G. and King's College London for funding. MGR acknowledges the Robert A. Welch Foundation (grant B-1093) for continued research support. The DFT calculations reported here were performed at UNT through CASCaM, which is an NSF-supported facility (CHE-1531468).

Appendix A. Supplementary material

CCDC 1861465 (for **2**) and CCDC 1861466 (for **3**) contain the supplementary crystallographic data for this paper. These data can be obtained free of charge from The Cambridge Crystallographic Data Centre via www.ccdc.cam.ac.uk/data_request/cif.

Table 1 Crystal data and structure refinement details

Complex	**2**	**3**
Empirical formula	$C_{29}H_{21}Fe_2O_5PS_2$	$C_{41}H_{32}Fe_2O_4P_2S_2$
Formula weight	656.25	897.33
Temperature (K)	150(2)	150(2)
Wavelength (Å)	0.71073	0.71073
Crystal system	orthorhombic	triclinic
Space group	*Pbca*	*P*-1
Unit cell dimensions		
a (Å)	17.2973(10)	14.310(3)
b (Å)	15.6070(9)	16.653(4)
c (Å)	20.9270(12)	18.478(4)
α (°)	90	115.075(3)
β (°)	90	94.809(4)
γ (°)	90	99.124(3)
Volume (Å^3)	5649.4(6)	3881.2(14)
Z	8	4
Density (calculated) (Mg/m^3)	1.543	1.536
Absorption coefficient (mm^{-1})	1.269	1.117
F(000)	2672	1832
Crystal size (mm^3)	0.26 × 0.13 × 0.13	0.28 × 0.26 × 0.08
Θ range for data collection (°)	2.79 to 28.30	2.48 to 28.34
Index ranges	$-22 \leq h \leq 22$, $-20 \leq k \leq 20$, $-27 \leq l \leq 26$	$-18 \leq h \leq 18$, $-21 \leq k \leq 21$, $-23 \leq l \leq 23$
Reflections collected	46753	32780
Independent reflections [R_{int}]	6896 [$R_{\mathrm{int}} = 0.0427$]	17593 [$R_{\mathrm{int}} = 0.0379$]
Max. and min. transmission	0.8524 and 0.7338	0.9159 and 0.7450
Data / restraints / parameters	6896 / 0 / 352	17593 / 0 / 955
Goodness of fit on F^2	1.056	1.022
Final *R* indices [$I > 2\sigma(I)$]	$R_1 = 0.0378$, $wR_2 = 0.0837$	$R_1 = 0.0512$, $wR_2 = 0.1339$
R indices (all data)	$R_1 = 0.0501$, $wR_2 = 0.0879$	$R_1 = 0.0740$, $wR_2 = 0.1484$
Largest diff. peak and hole (e. Å^{-3})	0.479 and –0.276	1.378 and –0.821

Peer-reviewed version available at *Inorganics* **2018**, *6*, 122; doi:10.3390/inorganics6040122

References

1. Tard, C.; Pickett, C.J. Structural and Functional Analogues of the Active Sites of the [Fe]-, [NiFe]-, and [FeFe]-Hydrogenases. *Chem. Rev.* **2009**, *109*, 2245-2274.
2. Sun, L.; Åkermark, B.; Ott, S. Iron hydrogenase active site mimics in supramolecular systems aiming for light-driven hydrogen production. *Coord. Chem. Rev.* **2005**, *249*, 1653-1663.
3. Evans, D.J.; Pickett, C.J. Chemistry and the hydrogenases. *Chem. Soc. Rev.* 2003, *32*, 268-275.
4. Georgakaki, I.P.; Thomson, L.M.; Lyon, E.J.; Hall, M.B.; Darensbourg, M.Y. Fundamental properties of small molecule models of Fe-only hydrogenase: computations relative to the definition of an entatic state in the active site. *Coord. Chem. Rev.* **2003**, *238−239*, 255-266.
5. Rauchfuss, T.B. Research on Soluble Metal Sulfides: From Polysulfido Complexes to Functional Models for the Hydrogenases. *Inorg. Chem.* **2004**, 43, 14-26.
6. Liu, X.; Ibrahim, S.K.; Tard, C.; Pickett, C.J. Iron-only hydrogenase: Synthetic, structural and reactivity studies of model compounds. *Coord. Chem. Rev.* **2005**, *249*, 1641-1652.
7. Lubitz, W.; Ogata, H.; Rüdiger, O.; Reijerse, E. Hydrogenases. *Chem. Rev.* **2014**, *114*, 4081-4148.
8. Peters, J.W.; Lanzilotta, W.N.; Lemon, B.; Seefeldt, L.C. X-ray Crystal Structure of the Fe-Only Hydrogenase (CpI) from *Clostridium pasteurianum* to 1.8 Angstrom Resolution. *Science* **1998**, *282*, 1853-1858.
9. Nicolet, Y.; Piras, C.; Legrand, P.; Hatchikian, C.E.; Fontecilla-Camps, J.C. *Desulfovibrio desulfuricans* iron hydrogenase: the structure shows unusual coordination to an active site Fe binuclear center. *Structure* **1999**, *7*, 13-23.
10. Li, Y.; Rauchfuss, T.B. Synthesis of Diiron(I) Dithiolato Carbonyl Complexes. *Chem. Rev.* **2016**, *116*, 7043-7077.
11. Apfel, U.-P.; Pétillon, F.Y.; Schollhammer, P.; Talarmin, J.; Weigand, W. *[FeFe] Hydrogenase Models: An Overview. In Bioinspired Catalysis*; Schollhammer, P., Weigand, W., Eds.; Wiley-VCH: Weinheim, Germany, **2014**.
12. Lansing, J.C.; Manor, B.C.; Rauchfuss, T.B. *Hydrogenase Models. Encyclopedia of Inorganic and Bioinorganic Chemistry* **2014**, 1-21.

Peer-reviewed version available at *Inorganics* **2018**, *6*, 122; doi:10.3390/inorganics6040122

13. Tschierlei, S.; Ott, S.; Lomoth, R. Spectroscopically Characterized Intermediates of Catalytic H_2 Formation by [FeFe]Hydrogenase Models. *Energy Environ. Sci.* **2011**, *4*, 2340-2352.
14. Felton, G.A.N.; Mebi, C.A.; Petro, B.J.; Vannucci, A.K.; Evans, D.H.; Glass, R.S.; Lichtenberger, D.L. Review of Electrochemical Studies of Complexes Containing the Fe_2S_2 Core Characteristic of [FeFe]-Hydrogenases Including Catalysis by These Complexes of the Reduction of Acids to Form Dihydrogen. *J. Organomet. Chem.* **2009**, *694*, 2681-2699.
15. Gloaguen, F. Electrochemistry of Simple Organometallic Models of Iron-Iron Hydrogenases in Organic Solvent and Water. *Inorg. Chem.* **2016**, *55*, 390-398.
16. Camara, J.M.; Rauchfuss, T.B. Mild Redox Complementation Enables H_2 Activation by [FeFe]-Hydrogenase Models. *J. Am. Chem. Soc.* **2011**, *133*, 8098-8101.
17. Camara, J.M.; Rauchfuss, T.B. Combining Acid-base, Redox and Substrate Binding Functionalities to Give a Complete Model for the [FeFe]-hydrogenase. *Nat. Chem.* **2012**, *4*, 26-30.
18. Greco, C. H_2 Binding and Splitting on a New-Generation [FeFe]-Hydrogenase Model Featuring a Redox-Active Decamethylferrocenyl Phosphine Ligand: A Theoretical Investigation. *Inorg. Chem.* **2013**, *52*, 1901-1908.
19. Ghosh, S.; Hogarth, G.; Hollingsworth, N.; Holt, K.B.; Kabir, S.E.; Sanchez, B.E. Hydrogenase biomimetics: $Fe_2(CO)_4(\mu\text{-dppf})(\mu\text{-pdt})$(dppf = 1,1’-bis(diphenylphosphino)ferrocene) both a proton-reduction and hydrogen oxidation catalyst. *Chem. Commun.* **2014**, *50*, 945-947.
20. Ghosh, S.; Rahaman, A.; Holt, K.B.; Nordlander, E.; Richmond, M.G.; Kabir, S.E.; Hogarth, G. Hydrogenase biomimetics with redox-active ligands: Electrocatalytic proton reduction by $[Fe_2(CO)_4(\kappa^2\text{-diamine})(\mu\text{-edt})]$ (diamine = 2,2′-bipy,1,10-phen). *Polyhedron* **2016**, *116*, 127-135.
21. Rauchfuss, T.B. Diiron Azadithiolates as Models for the [FeFe]-Hydrogenase Active Site and Paradigm for the Role of the Second Coordination Sphere, *Acc. Chem. Res.* **2015**, *48*, 2107-2116.
22. S. Youtao, K. Charreteur, J.-F. Capon, F. Gloaguen, F. Y. Pétillon, P. Schollhammer and J. Talarmin, J. Inorg. Biochem., 2010, 104, 1038–1042.

Peer-reviewed version available at *Inorganics* **2018**, *6*, 122; doi:10.3390/inorganics6040122

23. Adam, F.I., Hogarth, G.; Richards, I.; Sanchez, B.E. Models of the iron-only hydrogenase: Structural studies of chelating diphosphine complexes [$Fe_2(CO)_4$(μ-pdt)(κ^2-P,P′-diphosphine)]. *Dalton Trans.* **2007**, 2495-2498.
24. Adam, F.I.; Hogarth, G.; Richards, I. Models of the iron-only hydrogenase: Reactions of [$Fe_2(CO)_6$(μ-pdt)] with small bite-angle diphosphines yielding bridge and chelate diphosphine complexes [$Fe_2(CO)_4$(diphosphine)(μ-pdt)]. *J. Organomet. Chem.* **2007**, *692*, 3957–3968.
25. Adam, F.I.; Hogarth, G.; Kabir, S.E.; Richards, I. Models of the iron-only hydrogenase: Synthesis and protonation of bridge and chelate complexes [$Fe_2(CO)_4\{Ph_2P(CH_2)_nPPh_2\}$(μ-pdt)] (n=2–4) – evidence for a terminal hydride intermediate. *C. R. Chim.* **2008**, *11*, 890–905.
26. Ghosh, S.; Sanchez, B.E.; Richards, I.; M.N.; Holt, K.B.; Richmond, M.G.; Hogarth, G. Biomimetics of the [FeFe]-hydrogenase enzyme: Identification of kinetically favoured apical-basal [$Fe_2(CO)_4$(μ-H){κ^2-$Ph_2PC(Me_2)PPh_2$}(μ-pdt)]$^+$ as a proton-reduction catalyst, *J. Organomet. Chem.* **2016**, *812*, 247-258.
27. Ghosh, S.; G. Hogarth, G.; Hollingsworth, N.; Holt, K.B.; Richards, I.; Richmond, M.G.; Sancheza, B.E.; Unwin, D. Models of the iron-only hydrogenase: a comparison of chelate and bridge isomers of $Fe_2(CO)_4\{Ph_2PN(R)PPh_2\}$(μ-pdt) as proton-reduction catalysts. *Dalton Trans.* **2013**, *42*, 6775-6792
28. Ridley, F.; Ghosh, S.; Hogarth, G.; Hollingsworth, N.; Holt, K.B.; Unwin, D.G. Fluorinated models of the iron-only hydrogenase: An electrochemical study of the influence of an electron-withdrawing bridge on the proton reduction overpotential and catalyst stability. *J. Electroanal. Chem.* **2013**, *703*, 14-22.
29. Rana, S.; Ghosh, S.; Hossain, M.K.; Rahaman, A.; Hogarth, G.; Kabir, S.E. Hydrogenase biomimetics: Structural and spectroscopic studies on diphosphine-substituted derivatives of $Fe_2(CO)_6$(μ-edt) (edt = ethanedithiolate) and $Fe_2(CO)_6$(μ-tdt) (tdt = 1,3-toluenedithiolate). *Trans. Met. Chem.* **2016**, *41*, 933-942.
30. Ezzaher, S.; Capon, J.-F.; Gloaguen, F.; Pétillon, F.Y.; Schollhammer, P.; Talarmin, J. Electron-Transfer-Catalyzed Rearrangement of Unsymmetrically Substituted Diiron Dithiolate Complexes Related to the Active Site of the [FeFe]-Hydrogenases. *Inorg. Chem.* **2007**, *46*, 9863–9872.
31. Ezzaher, S.; Capon, J.-F.; Gloaguen, F.; Pétillon, F.Y.; Schollhammer, P.; Talarmin, J. Evidence for the Formation of Terminal Hydrides by Protonation of an Asymmetric Iron Hydrogenase Active Site Mimic. *Inorg. Chem.* **2007**, *46*, 3426-3428.

Peer-reviewed version available at *Inorganics* **2018**, *6*, 122; doi:10.3390/inorganics6040122

32. Ezzaher, S.; Capon, J.-F.; Dumontet, N.; Gloaguen, F.; Pétillon, F.Y.; Schollhammer, P.; Talarmin, J. Electrochemical study of the role of a H-bridged, unsymmetrically disubstituted diiron complex in proton reduction catalysis. *J. Electroanal. Chem.* **2009**, *626*, 161-170.
33. Justice, A.K.; Zampella, G.; Gioia, L.D.; Rauchfuss, T.B.; Vlugt, J.I. van der; Wilson, S.R. Chelate Control of Diiron(I) Dithiolates Relevant to the [Fe−Fe]- Hydrogenase Active Site. *Inorg. Chem.* **2007**, *46*, 1655-1664.
34. Wang, N.; Wang, M.; Liu, J.; Jin, K.; Chen, L.; Sun, L. Preparation, Facile Deprotonation, and Rapid H/D Exchange of the μ-Hydride Diiron Model Complexes of the [FeFe]-Hydrogenase Containing a Pendant Amine in a Chelating Diphosphine Ligand. *Inorg. Chem.* **2009**, *48*, 11551-11558.
35. Ezzaher, S.; Capon, J.-F.; Gloaguen, F.; Pétillon, F.Y.; Schollhammer, P.; Talarmin, J.; Kervarec, N. Influence of a Pendant Amine in the Second Coordination Sphere on Proton Transfer at a Dissymmetrically Disubstituted Diiron System Related to the $[2Fe]_H$ Subsite of $[FeFe]H_2ase$. *Inorg. Chem.* **2009**, *48*, 2-4.
36. Tard, C.; Liu, X.M.; Ibrahim, S.K.; Bruschi, M.; Gioia, L.D.; Davies, S.C.; Yang, X.; Wang, L.S.; Sawers, G.; Pickett, C.J. Synthesis of the H-cluster Framework of Iron-only Hydrogenase. *Nature* **2005**, *433*, 610-613.
37. Gimbert-Suriñach, C.; Bhadbhade, M.; Colbran, S.B. Bridgehead Hydrogen Atoms Are Important: Unusual Electrochemistry and Proton Reduction at Iron Dimers with Ferrocenyl-Substituted Phosphido Bridges. *Organometallics* **2012**, *31*, 3480-3491.
38. Greco, C.; Gioia, L.D. A Theoretical Study on the Enhancement of Functionally Relevant Electron Transfers in Biomimetic Models of [FeFe]-Hydrogenases. *Inorg. Chem.* **2011**, *50*, 6987-6995.
39. Orain, P.-Y.; Capon, J.-F.; Gloaguen, F.; Pétillon, F.Y.; Schollhammer, P.; Talarmin, J.; Zampella, G.; Gioia, L.D.; Roisnel T. Investigation on the Protonation of a Trisubstituted $[Fe_2(CO)_3(PPh_3)(\kappa^2\text{-phen})(\mu\text{-pdt})]$ Complex: Rotated versus Unrotated Intermediate Pathways. *Inorg. Chem.* **2010**, *49*, 5003-5008.
40. Ezzaher, S.; Orain, P.-Y.; Capon, J.-F.; Gloaguen, F.; Pétillon, F.; Roisnel, T.; Schollhammer, P.; Talarmin, J. First Insights into the Protonation of Dissymetrically Disubstituted Di-iron Azadithiolate Models of the $[FeFe]H_2ases$ Active Site. *Chem. Commun.* **2008**, 2547-2549.

41. Capon, J.-F.; Gloaguen, F.; Pétillon, F.Y.; Schollhammer, P.; Talarmin, J. Organometallics Diiron Complex Chemistry Related to the [2Fe]$_H$ Subsite of [FeFe]H$_2$ase. *Eur. J. Inorg. Chem.* **2008**, 4671-4681.
42. Orain, P.-Y.; Capon, J.-F.; Kervarec, N.; Gloaguen, F.; Pétillon, F.; Pichon, R.; Schollhammer, P.; Talarmin, J. Use of 1,10-Phenanthroline in Diiron Dithiolate Derivatives Related to the [Fe–Fe] Hydrogenase Active Site. *Dalton Trans.* **2007**, 3754-3756.
43. Roy, S.; Groy, T.L.; Jones, A.K. Biomimetic Model for [FeFe]-hydrogenase: Asymmetrically Disubstituted Diiron Complex with a Redox-active 2,2′-Bipyridyl Ligand. *Dalton Trans.* **2013**, 42, 3843-3853.
44. Bruschi, M.; Greco, C.; Fantucci, P.; Gioia, L.D. Structural and Electronic Properties of the [FeFe] Hydrogenase H-Cluster in Different Redox and Protonation States. A DFT Investigation. *Inorg. Chem.* **2008**, *47*, 6056-6071.
45. Schwab, D.E.; Tard, C.; Brecht, E.; Peters, J.W.; Pickett, C.J.; Szilagyi, R.K.; On the Electronic Structure of the Hydrogenase H-cluster. *Chem. Commun.* **2006**, 3696-3698.
46. Costa, T.; Schmidbaur, H. 1,8-Naphthalenediylhis(dimethylphosphane): Steric Influence on Methylation and Borylation. *Chem. Ber.* **1982**, *115*, 1374-1378.
47. Fenske, D.; Becher, H.J. Synthesis and Properties of Derivatives of 2,3-Bis(diphenylphosphino)maleic Anhydride as a Contribution to the Problem of Colour, Conjugation, and Complex Formation of this Class of Compounds. *Chem. Ber.* **1975**, *108*, 2115-2123.
48. Winter, A; Zsolnai, L.; Huttner, G. Dinuclear and Trinuclear Carbonyliron Complexes Containing 1,2- and 1,3-Dithiolato Bridging Ligands. *Z. Naturforsch* **1982**, *37b*, 1430-1436.
49. APEX2 Version 2.0-2, Bruker AXS Inc.: Madison, WI, **2005**.
50. SAINT Version 7.23A; Bruker AXS Inc.: Madison, WI, **2005**.
51. Sheldrick, G.M.; SADABS Version 2004/1, University of Göttingen, **2004**.
52. Program XS from SHELXTL package, V. 6.12, Bruker AXS Inc.: Madison, WI, **2001**.
53. Zhao, Y., Truhlar, D.G. *Theor. Chem. Acc.* 2008, *120*, 215-241.
54. Gaussian 09, Revision A.02, Frisch, M. J.; Trucks, G. W.; Schlegel, H. B.; Scuseria, G. E.; Robb, M. A.; Cheeseman, J. R.; Scalmani, G.; Barone, V.; Mennucci, B.; Petersson, G. A.; Nakatsuji, H.; Caricato, M.; Li, X.; Hratchian, H. P.; Izmaylov, A. F.; Bloino, J.; Zheng, G.; Sonnenberg, J. L.; Hada, M.; Ehara, M.; Toyota, K.;

Fukuda, R.; Hasegawa, J.; Ishida, M.; Nakajima, T.; Honda, Y.; Kitao, O.; Nakai, H.; Vreven, T.; Montgomery, J. A., Jr.; Peralta, J. E.; Ogliaro, F.; Bearpark, M.; Heyd, J. J.; Brothers, E.; Kudin, K. N.; Staroverov, V. N.; Kobayashi, R.; Normand, J.; Raghavachari, K.; Rendell, A.; Burant, J. C.; Iyengar, S. S.; Tomasi, J.; Cossi, M.; Rega, N.; Millam, J. M.; Klene, M.; Knox, J. E.; Cross, J. B.; Bakken, V.; Adamo, C.; Jaramillo, J.; Gomperts, R.; Stratmann, R. E.; Yazyev, O.; Austin, A. J.; Cammi, R.; Pomelli, C.; Ochterski, J. W.; Martin, R. L.; Morokuma, K.; Zakrzewski, V. G.; Voth, G. A.; Salvador, P.; Dannenberg, J. J.; Dapprich, S.; Daniels, A. D.; Farkas, Ö.; Foresman, J. B.; Ortiz, J. V.; Cioslowski, J.; Fox, D. J. Gaussian, Inc., Wallingford CT, 2009.

55. Dolg, M., Wedig, U., Stoll, H., Preuss, H. Energy-adjusted *ab initio* pseudopotentials for the second and third row transition elements. *J. Chem. Phys.* **1987,** *86***,** 866-872.

56. Bruce, M.I.; Humphrey, P.A.; Okucu, S.; Schmutzler, R.; Skelton, B.W.; White, A.H. Reactions of 1,8-Bis(diphenylphosphino)naphthalene with $Os_3(CO)_{12}$: C–H and C–P Bond Cleavage Reactions. *J. Organomet. Chem.* **2004**, *689*, 2415-2420.

57. Kabir, S.E.; Ahmed, F.; Ghosh, S.; Hassan, M.R.; Islam, M.S.; Sharmin, A.; Tocher, D.A.; Haworth, D.T.; Lindeman, S.V.; Siddiquee, T.A.; Bennett, D.W.; Hardcastle, K.I. Reactions of Rhenium and Manganese Carbonyl Complexes with 1,8-Bis(diphenylphosphino)naphthalene: Ligand Chelation, C–H and C–P Bond-cleavage Reactions. *J. Organomet. Chem.* **2008**, *693*, 2657-2665.

58. Kabir, S.E.; Rahman, A.F.M.M.; Parvin, J.; Malik, K.M.A. Reexamination of the Reactivity of Iron Carbonyls with 1,2-Ethanedithiol. *Indian J. Chem.* **2003**, *42A*, 2518-2522.

59. Ghosh, S.; Holt, K.B.; Kabir, S.E.; Richmond, M.G.; Hogarth, G. Electrocatalyic proton reduction catalyzed by the low-valent tetrairon-oxo cluster $[Fe_4(CO)_{10}(\kappa^2\text{-dppn})(\mu_4\text{-O})]^{2-}$ [dppn = 1,1'-bis(diphenylphosphino)naphthalene]. Dalton Trans. **2015**, *44*, 5160-5169.

60. Rose, M.J.; Gray, H.B.; Winkler, J.R. Hydrogen Generation Catalyzed by Fluorinated Diglyoxime−Iron Complexes at Low Overpotentials, J. Am. Chem. Soc. 134 (2012) 8310-8313.

61. Hu, X.; Brunschwig, B.S.; Peters, J.C. Electrocatalytic Hydrogen Evolution at Low Overpotentials by Cobalt Macrocyclic Glyoxime and Tetraimine Complexes. *J. Am. Chem. Soc.* **2007**, *129*, 8988-8998.

doi:10.20944/preprints201808.0477.v1

Peer-reviewed version available at *Inorganics* **2018**, *6*, 122; doi:10.3390/inorganics6040122

62. Jacobsen, G.M.; Yang, J.Y.; Twamley, B.; Wilson, A.D.; Bullock, R.M.; Rakowski-DuBois, M.; DuBois, D.L. Hydrogen Production Using Cobalt-based Molecular Catalysts Containing a Proton Relay in the Second Coordination Sphere. *Energy Environ. Sci.* **2008**, *1*, 167-174.
63. Jacobsen, G.M.; Yang, J.Y.; Twamley, B.; Wilson, A.D.; Bullock, R.M.; Rakowski-DuBois, M.; DuBois, D.L. Hydrogen Production Using Cobalt-based Molecular Catalysts Containing a Proton Relay in the Second Coordination Sphere. *Energy Environ. Sci.* **2008**, *1*, 167-174.
64. Helm, M.L.; Stewart, M.P.; Bullock, R.M.; DuBois, M.R.; DuBois, D.L. A Synthetic Nickel Electrocatalyst with a Turnover Frequency Above 100,000 s^{-1} for H_2 Production. *Science* **2011**, *333*, 863-866.

doi:10.20944/preprints201808.0477.v1

Peer-reviewed version available at *Inorganics* **2018**, *6*, 122; doi:10.3390/inorganics6040122

Table of Contents Entry

Hydrogenase biomimetics with redox-active ligands: Synthesis, structure and electrocatalytic studies on $Fe_2(CO)_4(\kappa^2$-dppn)(μ-edt) (edt = ethanedithiolate; dppn = 1,8-bis(diphenylphosphino)naphthalene)

Shishir Ghosh,* Shahed Rana, Nathan Hollingsworth, Michael G. Richmond, Shariff E. Kabir and Graeme Hogarth*

$[Fe_2(CO)_4(\kappa^2$-dppn)(μ-edt)] bearing a redox-active dppn ligand has been synthesized and found to be a high-performing electrocatalyst for proton-reduction.